Ferroelectric phases of dipolar hard spheres

J. J. Weis and D. Levesque
Laboratoire de Physique Théorique et Hautes Energies, Bâtiment 211, Université de Paris–Sud, 91405 Orsay Cedex, France
(Received 13 April 1993)

The phase diagram of strongly dipolar hard spheres in the dense fluid and solid regions is investigated by Monte Carlo simulations. Main emphasis is given to the analysis of the stability of body-centered-tetragonal, face-centered-cubic, and body-centered-orthorhombic crystal phases. The existence of ferroelectric phases is demonstrated in agreement with the findings of previous simulations for dipolar soft spheres by Wei and Patey [Phys. Rev. A **46**, 7783 (1992)].

PACS number(s): 64.70.Md, 77.80.−e, 82.20.Wt

I. INTRODUCTION

Strong dipolar interactions play an important role in many physical systems of technological interest including ferrofluids (stable colloidal dispersions of monodomain magnetic particles) [1], electrorheological fluids (colloidal suspensions of highly polarizable particles in a solvent with low dielectric constant) [2], magnetic holes (colloidal spheres dispersed in a ferrofluid) [3], etc. Yet the phase diagram of even the simplest model for describing these systems, namely, dipolar hard spheres, is still imperfectly known. Part of this gap has been filled recently through Monte Carlo (MC) and molecular-dynamics simulations of both the low-density [4] and high-density [5] regions of the phase diagrams of strongly interacting dipolar hard spheres and the closely related system of dipolar soft spheres [6]. The former were directed towards the search of a liquid-gas transition, the latter towards an investigation of the orientationally ordered phases at high density. Quite interestingly, evidence was obtained for the existence of ferroelectric ordering in the fluid and solid phases. The aim of this paper is to present the results of detailed MC simulations completing those briefly reported in Ref. [5]. Most of our MC calculations were performed at the fixed reduced temperature $T^*=1/\mu^{*2}$, where

$$\mu^*=(\mu^2/kT\sigma^3)^{1/2}=2.5$$

(μ is the dipole moment, T the temperature, σ the hard-sphere diameter, and k the Boltzmann constant), and cover the density range $\rho^*=\rho\sigma^3=0.7-1.2$, from the dense fluid to the solid. A few additional calculations were made for the higher dipole moment $\mu^*=3$. As already remarked in Refs. [5,6], the orientational behavior of the dipole moments will depend sensitively on the boundary conditions of the system. This is a consequence of the well-known fact that, due to the long range of the dipolar interaction, the local electric field includes contributions from the system's surface. Two boundary conditions have been considered: in one case the system is surrounded by a perfectly conducting medium (i.e., of infinite dielectric constant $\epsilon'=\infty$), and in the other by vacuum ($\epsilon'=1$). Only in the first case will the system exhibit a net polarization; in the latter case there will be two or more domains polarized in different directions so that the global polarization of the system is zero.

The remainder of the paper is organized as follows: In Sec. II we give technical details of the Monte Carlo calculations and define correlation functions which are useful to characterize the orientational order. The results for the fluid and solid phases are given in Sec. III and are discussed in Sec. IV.

II. MONTE CARLO SIMULATIONS

Most of the simulations were performed in the isobaric-isothermal (NpT) ensemble and, in a few cases, in the canonical (NVT) ensemble [7], using a parallelepipedic (NpT) or cubic (NVT) simulation cell repeated periodically in space, and the long-range dipolar interactions were accounted for using the Ewald method [7,8]. The Hamiltonian of the system is

$$H=-\tfrac{1}{2}\sum_{i\neq j}v_{ij}-\tfrac{1}{2}\sum_{i,j}\sum_{n}{}'(\boldsymbol{\mu}_i\cdot\nabla)(\boldsymbol{\mu}_j\cdot\nabla)\times\frac{\operatorname{erfc}(\alpha|\mathbf{r}_j-\mathbf{r}_i+\overleftrightarrow{h}\cdot\mathbf{n}|)}{|\mathbf{r}_j-\mathbf{r}_i+\overleftrightarrow{h}\cdot\mathbf{n}|}+\frac{1}{2\pi V}\sum_{\mathbf{k}\neq 0}\frac{4\pi}{\mathbf{k}^2}e^{-\mathbf{k}^2/4\alpha^2}F(\mathbf{k})F^*(\mathbf{k})-\sum_i\frac{2\alpha^3\mu_i^2}{3\sqrt{\pi}}+\frac{2\pi}{(2\epsilon'+1)V}\mathbf{M}^2\,, \tag{1}$$

where v_{ij} is the hard-sphere potential satisfying

$$v_{ij}=\begin{cases}\infty & \text{if } |\mathbf{r}_j-\mathbf{r}_i|<\sigma\\ 0 & \text{if } |\mathbf{r}_j-\mathbf{r}_i|>\sigma\end{cases} \tag{2}$$

and

$$F(\mathbf{k})=\sum_i\mathbf{k}\cdot\boldsymbol{\mu}_i e^{i\mathbf{k}\cdot\mathbf{r}_i}\,. \tag{3}$$

$\mathbf{M}=\sum_i\boldsymbol{\mu}_i$ is the total dipole moment of the system.

In Eq. (1), $\mathbf{r}_i$ denotes the position of dipole moment $\boldsymbol{\mu}_i$, ϵ' the dielectric constant of the medium surrounding a large sphere of cell replica, and erfc the complementary error function, and the prime in the sum over

$\mathbf{n}=(n_x,n_y,n_z)$, n_x,n_y,n_z integers, indicates that $i\neq j$ for $\mathbf{n}=0$. The diagonal matrix

$$\overleftrightarrow{h}=\begin{bmatrix} L_x & 0 & 0 \\ 0 & L_y & 0 \\ 0 & 0 & L_z \end{bmatrix} \tag{4}$$

has elements equal to the lengths of the edges of the simulation cell. The volume of the simulation cell is $V=L_xL_yL_z$. A vector $\mathbf{k}$ in reciprocal space is of the form $\mathbf{k}=2\pi\,{}^t\overleftrightarrow{h}^{-1}\cdot\mathbf{n}$, where ${}^t\overleftrightarrow{h}^{-1}$ denotes the transpose of the inverse of $\overleftrightarrow{h}$. The value of the parameter α was chosen such that $\alpha L_{\min}\simeq 5.75$, where

$$L_{\min}=\min(L_x,L_y,L_z)\ .$$

With this value the sum in the second term of the right-hand side (rhs) of Eq. (1) can be restricted to the term $\mathbf{n}=0$. This term was evaluated by summing all interactions inside the simulation box. The sum in reciprocal space extends over all values of $\mathbf{k}$ such that $|\mathbf{n}|^2\leq n_{\max}^2=36$. The present choice of the parameters $n_{\max}^2$ and α guarantees an accurate evaluation of the dipole-dipole energy [9]. The two different boundary conditions considered in this work correspond to $\epsilon'=1$ (vacuum) and $\epsilon'=\infty$ (conducting medium) in Eq. (1), respectively. In the first case the last term in the rhs of Eq. (1) represents the contribution to the energy from the depolarizing field due to the surface charges induced on the spherical boundary; in the second case this term vanishes (surface charges are absorbed by the conducting medium).

In the NpT ensemble, the MC sampling consisted, in cyclic order, of the displacements of the N hard-sphere centers and the rotations of the N dipole moments, followed by a volume change corresponding to an independent scaling of the lengths of the three sides of the simulation cell.

The possible occurrence of an orientational order was established from the nonvanishing of the order parameter S [10] defined as the average value of the largest eigenvalue of the second-rank tensor:

$$\overleftrightarrow{Q}=\frac{1}{N}\sum_{i=1}^{N}\tfrac{1}{2}(3\hat{\mathbf{u}}_i\hat{\mathbf{u}}_i-\overleftrightarrow{I})\ , \tag{5}$$

where $\hat{\mathbf{u}}_i$ is a unit vector along the dipole moment. The polarization of the system is calculated as the average value of

$$P=\frac{1}{N}\left|\sum_{i=1}^{N}\hat{\mathbf{u}}_i\cdot\hat{\mathbf{e}}\right|\ , \tag{6}$$

where $\hat{\mathbf{e}}$ denotes a unit vector in the direction of the instantaneous eigenvector associated with the largest eigenvalue of $\overleftrightarrow{Q}$ (i.e., the director, in the language of liquid-crystal theory). Information on structural ordering was obtained by calculating a number of correlation functions for the centers of mass of the spheres. Useful to identify crystal or columnar ordering (provided the crystal or columnar symmetry axes lie along the axes of the simulation cell) are the functions

$$f(i\Delta x_\alpha)=\frac{\left\langle\sum_{j=0}^{m}n(j\Delta x_\alpha)n((i+j)\Delta x_\alpha)\right\rangle}{m\rho^{*2}A_{\beta\gamma}^2\Delta x_\alpha^2}\quad(i\neq 0)\ , \tag{7}$$

where $n(x_\alpha)$ is the number of hard spheres having the x_α coordinate ($x_\alpha=x,y$, or z) of their centers in the interval $(x_\alpha,x_\alpha+\Delta x_\alpha)$, $m=L_\alpha/\Delta x_\alpha$ (recall that L_α is the length of the simulation cell in the α direction), $A_{\beta\gamma}=L_\beta L_\gamma$, and $\Delta x_\alpha=0.02\sigma$. For example, in the presence of a crystal structure, the functions $f(x)$, $f(y)$, and $f(z)$ will oscillate with periods corresponding to the lattice spacings of the crystal.

When the system orients in a preferred direction, the spatial arrangement can be further analyzed by considering the longitudinal correlation function $g_\parallel$ defined as

$$g_\parallel(r_\parallel)=\frac{\left\langle\sum_{i,j(i\neq j)}\delta(r_{ij,\parallel}-r_\parallel)\theta(\sigma/2-r_{ij,\perp})\right\rangle}{N\rho^*\pi(\sigma/2)^2}\ , \tag{8}$$

where $r_{ij,\parallel}=|\mathbf{r}_{ij}\cdot\hat{\mathbf{e}}|$ and $r_{ij,\perp}=|\mathbf{r}_{ij}-(\mathbf{r}_{ij}\cdot\hat{\mathbf{e}})\hat{\mathbf{e}}|$ are components of the interparticle vector $\mathbf{r}_{ij}$ parallel and perpendicular to the director $\hat{\mathbf{e}}$. From definition (8) it is apparent that $g_\parallel$ involves only particles inside a cylindrical volume of radius $\sigma/2$ and axis parallel to the director. (Note that this definition differs from that of Ref. [6] in which all particles of the system are involved.) It is clear that $g_\parallel$ will be particularly valuable to identify chain formation along the direction of alignment of the dipole moments. Finally, we calculated the correlation functions

$$g^{000}(r)=\frac{\left\langle\sum_{i,j(i\neq j)}\delta(r-|\mathbf{r}_{ij}|)\right\rangle}{N4\pi\rho^*r^2}\ , \tag{9a}$$

$$h^{110}(r)=3\frac{\left\langle\sum_{i,j(i\neq j)}\delta(r-|\mathbf{r}_{ij}|)\mathbf{u}_i\cdot\mathbf{u}_j\right\rangle}{N4\pi\rho^*r^2}\ , \tag{9b}$$

$$h^{112}(r)=\frac{3}{2}\frac{\left\langle\sum_{i,j(i\neq j)}\delta(r-|\mathbf{r}_{ij}|)[3(\mathbf{u}_i\cdot\hat{\mathbf{r}}_{ij})(\mathbf{u}_j\cdot\hat{\mathbf{r}}_{ij})-\mathbf{u}_i\cdot\mathbf{u}_j]\right\rangle}{N4\pi\rho^*r^2}\ , \tag{9c}$$

$$h^{220}(r)=\frac{5}{2}\frac{\left\langle\sum_{i,j(i\neq j)}\delta(r-|\mathbf{r}_{ij}|)[3(\mathbf{u}_i\cdot\mathbf{u}_j)^2-1]\right\rangle}{N4\pi\rho^*r^2}\ , \tag{9d}$$

where $\hat{\mathbf{r}}_{ij}=\mathbf{r}_{ij}/|\mathbf{r}_{ij}|$. In an orientationally isotropic system these correlation functions can be identified as the projections of the pair distribution function $g(12)$ on rotational invariants [11]. In the nematic phase these functions give only an indication of the spatial extension of the dipolar correlations. In particular, we can note that, as $r\to\infty$ [6],

$$h^{110}(r)\sim 3P^2\ , \tag{10a}$$

$$h^{220}(r)\sim 5S^2\ . \tag{10b}$$

In the NpT calculations the pressure is an input value. In the NVT calculations it is most easily obtained from the

virial theorem and can be expressed as the sum of a hard-core term and the dipole-dipole energy according to the equation

$$\frac{p_{\rm vir}}{\rho kT}=\frac{p_{\rm HC}}{\rho kT}+\frac{U_d}{NkT}\ . \tag{11}$$

In our simulations the hard-core contribution to the pressure was calculated by the method of Perram and Wertheim [12] (devised for ellipsoids but applying trivially in the case of hard spheres). In the NpT calculations comparison between the virial and external pressures has served as a test of the convergence of the results.

III. RESULTS

It will be convenient to present results obtained for the two boundary conditions separately. We first consider the case where the system is surrounded by a conducting medium; in Sec. III B we will show how these results are modified when the surrounding medium is replaced by vacuum.

A. $\epsilon'=\infty$

In the fluid region, a series of calculations has been carried out at constant densities $\rho^*=0.7$, 0.8, 0.86, and 0.9, arranging the particles ($N=500$) initially on a perfect fcc lattice with random orientations of the dipole moments. In all cases the crystal structure melted rapidly (vanishing of the translational order parameter $\rho_{\mathbf{k}}=\sum_i e^{i\mathbf{k}\cdot\mathbf{r}_i}$, where $\mathbf{k}$ is the smallest vector in reciprocal space) and a preferred orientation of the molecules, indicated by a nonzero value of the order parameter S, developed slowly, typically within a "time" span of about 40 000 to 50 000 trial moves per particle. After such a period, the system was assumed to be equilibrated and thermodynamic and structural data were collected for another period of 40 000–100 000 moves per particle. These results are summarized in Table I. The order parameter increases over the density range $\rho^*=0.7$–0.9 from 0.08 to ~ 0.55, its saturation value. More remarkably, the polarization is also found to be nonzero, so that we are in the presence of a ferroelectric nematic phase (the term nematic being used to indicate that there is no positional long-range order). The polarization increases sharply, reaching saturation ($P\sim 0.80$) at $\rho^*\simeq 0.85$. These results are in excellent agreement with the soft-sphere results of Wei and Patey [6].

The reduced pressure $p^*=p\sigma^3/\epsilon$ is shown in Fig. 1. The pressure values result from a compensation between a large hard-core contribution $p^*_{\rm HC}$ and a large negative energy value [cf. Table I and Eq. (11)]. Fluid states with density higher than 0.9 could only be obtained by starting from a bcc lattice (the fcc lattice transformed into a mechanically stable orthorhombic structure; see below). This gives some indication that the high-density ferroelectric-fluid region might in fact be metastable. In this respect it is worth recalling that pure hard spheres freeze at the density $\rho^*=0.943$ and melt at $\rho^*=1.04$ [13].

The pair-correlation-function projections at $\rho^*=0.90$ are shown in Fig. 2. In regard to these, the following points can be noticed: h^{110} and h^{112} decay to constant values at large r, as required for a ferroelectrically ordered system [Eq. (10)]. As all dipole moments are aligned (on average) in the same direction, h^{110} is positive and its structural information content is similar to that of the angle-averaged pair distribution function g^{000}. The projection h^{112} presents a negative region with minimum near $r\simeq 1.16\sigma$, indicating average repulsive interactions at these distances. Evidence for this feature has also been given for soft dipolar spheres [6]. It is also present in the solid phase (see below), but not in the isotropic phase, revealing some similarity of the structural properties of the nematic phase with those of the solid. All projections show a small cusp at $r=2\sigma$, typical of dimer formation. This structure is likely to be due to partial memory of the chain formation occurring in the solid phase (see below). Finally, a snapshot of a dipole configuration at $\rho^*=0.84$ and $\mu^*=3$ (projection on the yz plane of the simulation cell) clearly illustrates (Fig. 3) the ferroelectric behavior of this fluid state.

Let us now turn to the discussion of the solid-phase results. To our knowledge, the most stable structure of dipolar hard spheres is not known. Ideally, one would thus like to apply a simulation method in which the preferred crystal structure can adapt to the interaction potential. This is only possible if the basic simulation cell can vary both in volume *and* in shape. Although such a method is available (see Ref. [14] for its original derivation and Ref. [15] for its extensions to MC simulations), its application to long-range electrostatic potentials causes practical problems related to an economical evaluation of the Ewald potential [the need to recalculate the reciprocal-space contribution in Eq. (1) for each new cell shape]. For this reason we limited ourselves to an isobaric-isothermal MC sampling method in which the lengths of the cell edges are varied (independently in the three directions) but their directions kept mutually orthogonal.

The stability of two lattice structures, body-centered tetragonal (bct) and face-centered cubic (fcc), has been investigated. The former has been suggested by the work of Wei and Patey [6] as well as by theoretical analysis of structures in electrorheological (ER) fluids [16–19]; the latter is believed to be the most stable structure of high-density hard spheres [20] (although the free-energy difference between fcc ad hexagonal close-packed structures is extremely small [21]).

1. bct lattice

As already indicated, a bct crystal structure is believed to form in ER fluids when subject to an applied electric field [16]. ER fluids are colloidal suspensions of highly polarizable particles in a weakly polarizable solvent of low dielectric constant. When placed between two planar electrodes, such systems, for a moderately high electric field, first form chains which then coalesce to form thick columns [22, 2]. It has been argued recently [16] that the resulting solid structure inside these columns might be a bct lattice structure with convential lattice vectors $\mathbf{a}=(\sqrt{6}/2)\sigma\hat{\mathbf{x}}$, $\mathbf{b}=\sqrt{6}/2\sigma\hat{\mathbf{y}}$, and $\mathbf{c}=\sigma\hat{\mathbf{z}}$. This prediction

is based on ground-state energy calculations [16] for a model of perfect, infinitely long chains of dipolar spheres and seems to be supported by two-dimensional MC calculations (simulated annealing) [17] as well as laser diffraction experiments of small glass spheres in silicone oil [23].

A series of MC calculations, covering the density range $\rho^*=0.95-1.20$, has been performed starting from an initial perfect bct lattice with lattice vectors $\mathbf{a}=(\sqrt{6}/2)\sigma\hat{\mathbf{x}}$, $\mathbf{b}=(\sqrt{6}/2)\sigma\hat{\mathbf{y}}$, and $\mathbf{c}=\sigma\hat{\mathbf{z}}$. A nearly cubic simulation cell was obtained by taking six lattice planes in the x and y directions, respectively, and eight planes in the z direction, resulting in a total of 576 particles. The initial dipole moments of the spheres were chosen randomly. The cell dimensions were then expanded uniformly in all three directions to obtain the desired density. Initially, the hard spheres are thus not in contact along the z direction. In all cases (summarized in Table I), the system polarized rapidly in the z direction (typically within 10 000–20 000 trial moves per particle, and thus much faster than in the

TABLE I. Thermodynamic properties (reduced density ρ^*, pressure p^*, dipolar energy U_d/NkT) and order parameters (S, nematic order parameter; P polarization) of dipolar hard spheres at $\mu^*=2.5$ in the fluid (nematic), face-centered-cubic (fcc), tetragonal I (bct), and orthorhombic I (bco) phases. n denotes the number of trial moves per particle after equilibration. In the isothermal-isobaric ensemble (NpT) MC method, p^* is the external pressure; in the canonical ensemble (NVT) MC method, p^* is the virial pressure calculated according to Eq. (11). p^*_{HC} is the hard-core contribution to the virial pressure.

N	MC method	ϵ'	n	ρ^*	p^*	p^*_{HC}	U_d/NkT	S	P
				Fluid					
500	NVT	∞	40 000	0.70	1.13	12.4	−11.80	0.08	0.17
500	NVT	∞	100 000	0.80	1.96	13.9	−12.47	0.38	0.70
500	NVT	∞	100 000	0.86	2.87	15.1	−12.97	0.42	0.78
500	NVT	∞	80 000	0.90	3.66	16.1	−13.07	0.52	0.80[a]
500	NVT	∞	80 000	0.90	3.52	16.1	−13.13	0.56	0.82[b]
432	NpT	∞	200 000	0.974	6.4	18.9	−13.31	0.56	0.82[c]
500	NpT	1.0	60 000	0.916	4.2	16.8	−12.99	0.30	0.0
500	NVT	1.0	40 000	1.00	7.85	20.2	−13.35	0.10	0.0
500	NVT	∞	100 000	0.84	1.10	20.3	−20.03	0.65	0.86[d]
500	NVT	1.0	120 000	0.84	1.68	20.6	−19.60	0.20	0.0[d]
				bct					
576	NpT	∞	20 000	1.18	10.6	22.2	−15.39	0.80	0.93
576	NpT	∞	90 000	1.077	4.5	18.2	−15.15	0.81	0.93
576	NpT	∞	140 000	1.005	2.4	16.2	−14.74	0.80	0.93
576	NpT	∞	60 000	0.96	1.5	15.1	−14.40	0.81	0.93
576	NpT	1.0	40 000	1.181	10.6	21.6	−15.00	0.72	0.0
				fcc					
500	NVT	∞	40 000	1.20	10.7	23.0	−15.10	0.50	0.75
500	NpT	∞	60 000	1.138	6.5	19.5	−14.81	0.44	0.78
500	NpT	∞	100 000	1.084	4.2	17.6	−14.50	0.43	0.77
500	NpT	∞	60 000	1.024	3.1	16.0	−14.10	0.42	0.76
500	NVT	1.0	40 000	1.20	10.2	22.0	−14.50	0.06	0.0
500	NpT	1.0	40 000	1.143	6.4	18.7	−14.10	0.05	0.0
500	NpT	1.0	60 000	1.069	4.2	17.1	−13.73	0.13	0.0
				bco					
500	NpT	∞	40 000	1.066	4.2	17.7	−14.99	0.81	0.93
500	NpT	∞	40 000	1.01	2.0	15.4	−14.50	0.80	0.93
500	NVT	∞	50 000	0.95	0.38	13.2	−13.83	0.78	0.92[e]
500	NpT	∞	50 000	0.947	0.38	13.4	−13.89	0.78	0.92[f]
500	NVT	∞	60 000	0.92	0.18	12.6	−13.45	0.74	0.90

[a]Run started from a fcc lattice.
[b]Run started from the final configuration of the bco structure at $\rho^*=0.92$.
[c]Run started from a body-centered-cubic (bcc) lattice at $\rho^*=1.05$.
[d]Results for $\mu^*=3$.
[e]Run started from a fcc lattice at $\rho^*=0.95$ (NVT).
[f]Run started from the final configuration of the preceding run at $\rho^*=0.95$ but using NpT MC sampling.

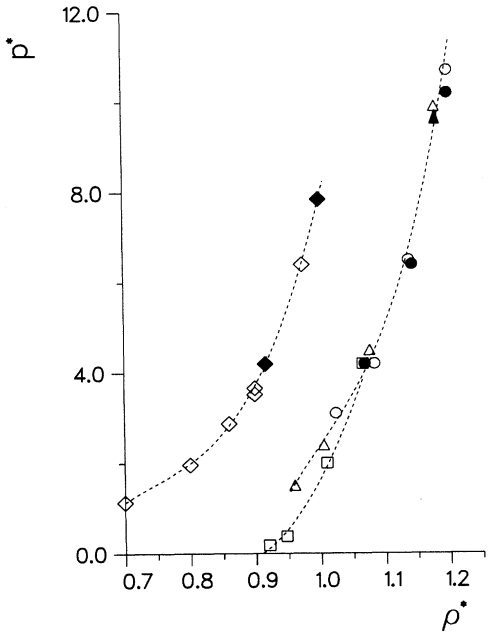

FIG. 1. The reduced pressure p^* as a function of density for dipolar hard spheres at $\mu^*=2.5$. The fluid-state results are represented by diamonds. The solid-state results are shown as circles (fcc lattice), triangles (bct lattice), or squares (bco lattice). The open and solid symbols denote results obtained with $\epsilon'=\infty$ and $\epsilon'=1$, respectively.

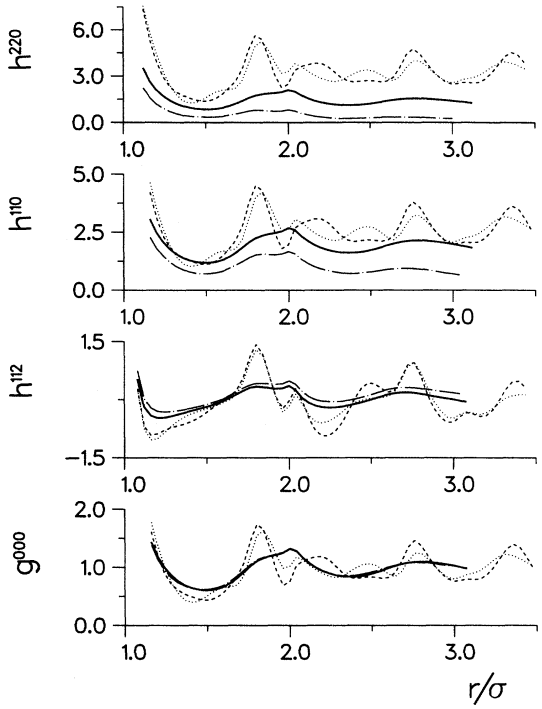

FIG. 2. Projections of the pair distribution function of dipolar hard spheres at $\mu^*=2.5$. Solid line: $\rho^*=0.9$, $\epsilon'=\infty$ (fluid); contact values are $g^{000}=8.4$, $h^{112}=10.3$, $h^{110}=19.0$, and $h^{220}=18.5$. Dotted line: $\rho^*=1.01$, $\epsilon'=\infty$ (bco); contact values are $g^{000}=7.2$, $h^{112}=9.7$, $h^{110}=18.7$, and $h^{220}=23.7$. Dashed line: $\rho^*=1.005$, $\epsilon'=\infty$ (bct); contact values are $g^{000}=7.5$, $h^{112}=9.6$, $h^{110}=19.6$, and $h^{220}=25.1$. Dot-dashed line: $\rho^*=0.916$, $\epsilon'=1$ (fluid); contact values are $g^{000}=8.8$, $h^{112}=10.8$, $h^{110}=17.4$, and $h^{220}=14.8$.

fluid phase), and the simulation cell contracted in this direction to yield a lattice spacing $c=|\mathbf{c}|\sim 1.025\sigma$, practically independent of density. The structure can thus be interpreted as resulting from formation of chains in the z direction. The lattice spacings a and b in the x and y directions are equal at high density ($a\simeq b\simeq 1.283\sigma$, for $\rho^*=1.18$) but get slightly different on lowering the density (for example, $a/b\simeq 1.07$ at $\rho^*=1.005$).

A typical angle-averaged pair distribution function g^{000} (at $\rho^*=1.077$), demonstrating the bct structure, is shown in Fig. 4. The orientational structure of the dipoles at $\rho^*=1.077$ is illustrated in Fig. 5 by the projections of an instantaneous configuration of the dipole moments on the xy, xz, and yz planes of the simulation cell. The polarization of the system in the (minus) z direction is manifest. To show more clearly the chain formation, projections on the xz plane of the particles in one lattice plane (chosen parallel to the projection plane) are shown as well. The result is striking (Fig. 6). The order parameters in the bct phase are quite high, $S\simeq 0.80$ and $P\simeq 0.93$, independent of density (cf. Table I).

2. *fcc lattice*

Next we investigated the stability of the fcc phase. A first simulation was made for a system of 500 hard spheres, at density $\rho^*=1.2$ ($p^*=10.7$), with centers located initially on a perfect fcc lattice and orientations of the dipole moments chosen randomly. Again, it took a relatively short "time" ($\sim 10\,000$ trial moves per particle) for the system to polarize in the direction of one of the

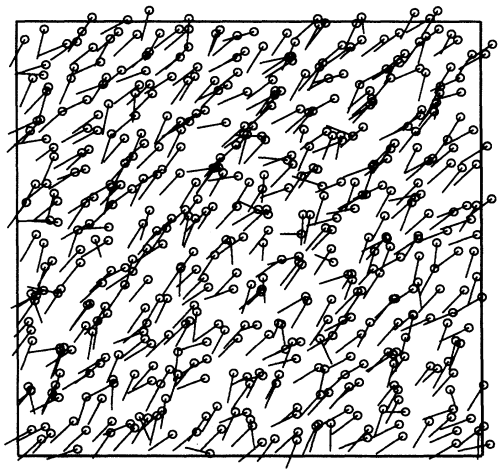

FIG. 3. Snapshot of a configuration of 500 dipolar hard spheres at $\rho^*=0.84$, $\mu^*=3$, and $\epsilon'=\infty$ (fluid) (projection of the dipole moments on the xy plane of the periodic box). The dipole moments are represented by thin lines of length 0.6σ. The hard-sphere centers are in the middle of the lines. The circles indicate the head of the dipole moments. The dimensions of the simulation cell are $L_x=L_y=L_z=8.41\sigma$.

cell axes. Subsequent runs at pressures $p^*=6.5$, 4.2, and 3.1 were made using as a starting configuration the final configuration (possibly randomizing the orientations) of the previous run at a higher pressure and scaling uniformly the cell dimensions and particle positions to obtain approximately the expected density.

The fcc lattice structure is found to be mechanically stable until a density $\rho^* \simeq 1.02$. An angle-averaged pair distribution function (PDF) g^{000}, typical of a fcc structure, is shown in Fig. 4(a) for $\rho^*=1.084$. For all states considered, the simulation cell remained practically cubic; in particular, no contraction in the direction of the average polarization was observed. However, the hard-sphere centers are more strongly localized in the direction of polarization than in the perpendicular directions, as is apparent from Fig. 7 which shows the functions $f(x)$, $f(y)$, and $f(z)$ [Eq. (7)] for $\rho^*=1.138$. Here, $f(z)$ (the polarization is along the z axis) is seen to have higher and sharper peaks than $f(x)$ or $f(y)$. How the dipole moments orient in the fcc phase can be inferred from a snapshot of the system at density 1.138 (Fig. 8). We note that, in lattice planes perpendicular to the direction of polarization (z axis), the dipole moments orient nearly parallel, making an angle of $\sim 40°$ with the z axis. Moreover, the direction of orientation of the dipole moments varies helically from one lattice plane to the other (spaced

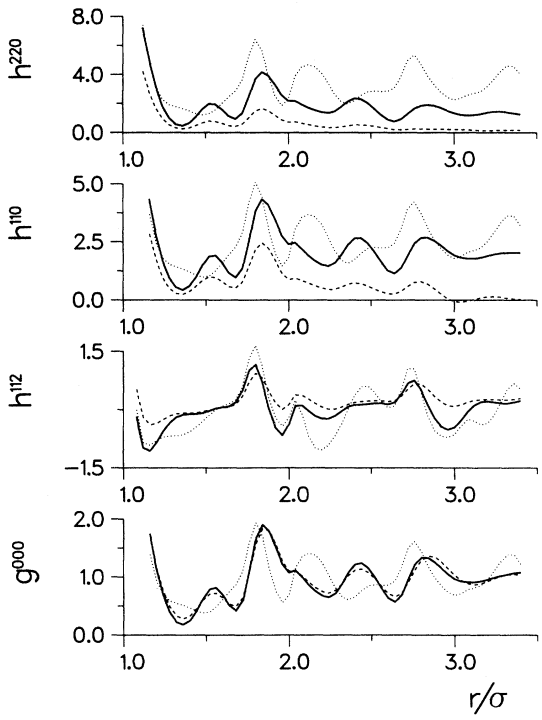

FIG. 4. Projections of the pair distribution function of dipolar hard spheres at $\mu^*=2.5$. Solid line: $\rho^*=1.084$, $\epsilon'=\infty$ (fcc); contact values are $g^{000}=7.6$, $h^{112}=8.5$, $h^{110}=19.1$, and $h^{220}=22.2$. Dashed line: $\rho^*=1.069$, $\epsilon'=1$ (fcc); contact values are $g^{000}=8.0$, $h^{112}=9.2$, $h^{110}=21.2$, and $h^{220}=27.6$. Dotted line: $\rho^*=1.077$, $\epsilon'=\infty$ (bct); contact values are $g^{000}=7.6$, $h^{112}=7.6$, $h^{110}=15.8$, and $h^{220}=15.3$.

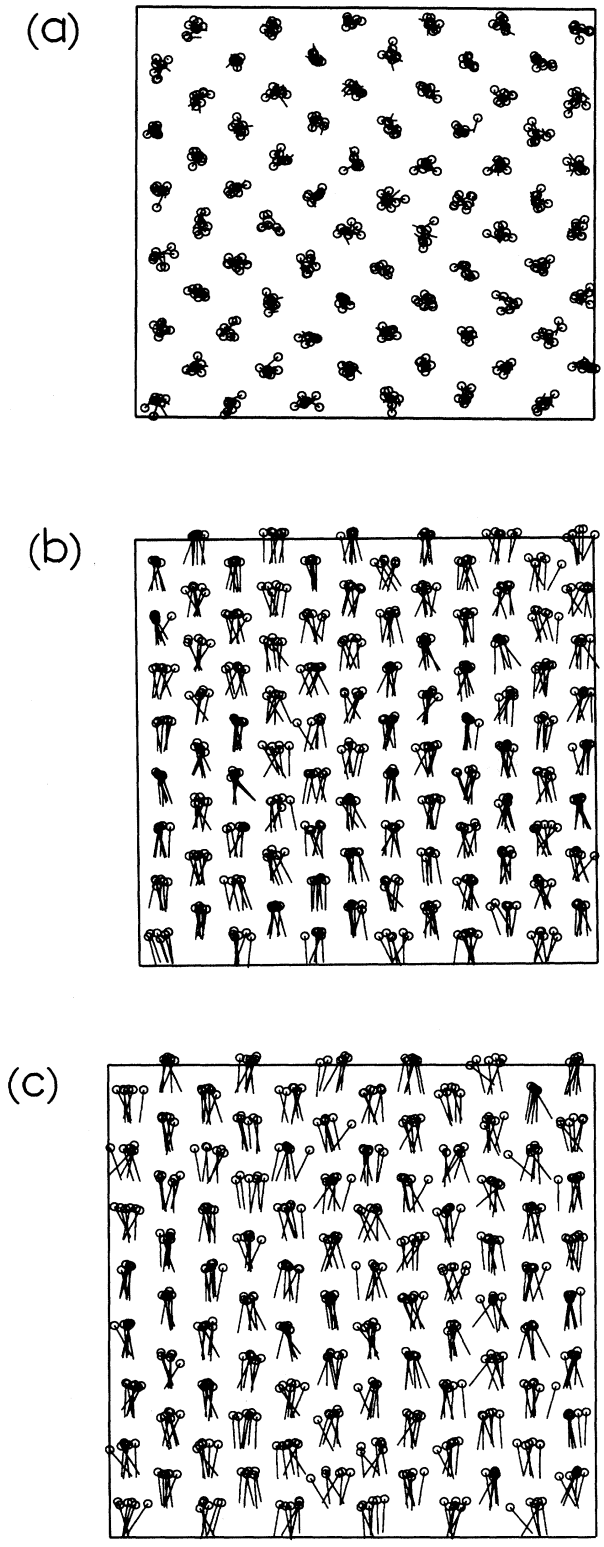

FIG. 5. Snapshot of a configuration of 576 dipolar hard spheres at $\rho^*=1.077$, $\mu^*=2.5$, and $\epsilon'=\infty$ (bct phase). Projections of the dipole moments on the (a) xy, (b) xz, and (c) yz planes of the periodic simulation cell. The symbols are as in Fig. 3. The dimensions of the simulation cell are $L_x=8.24\sigma$, $L_y=7.90\sigma$, and $L_z=8.22\sigma$.

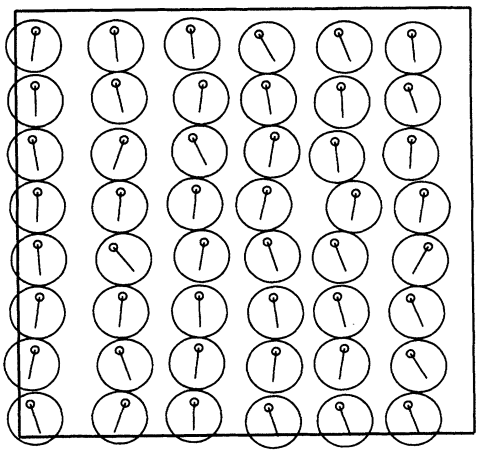

FIG. 6. Same as Fig. 5 but for hard spheres in one lattice plane parallel to the xy plane of the simulation box only. This snapshot clearly demonstrates the formation of chains along the z axis of the bct lattice. The dimensions of the simulation cell are $L_x=8.24\sigma$, $L_y=7.90\sigma$, and $L_z=8.22\sigma$.

by $c/2$) with one full turn of the helix over the cell length L_z, as required by the periodic boundary conditions. This pattern is observed in the whole density range over which the fcc is stable.

For this peculiar orientational order we can expect the order parameters to be smaller than for the bct structure. This is indeed the case: in the fcc phase one has, typically, $S\simeq 0.5$ and $P\simeq 0.75$ (cf. Table I). In contrast, the pressure does not differ from that of the bct phase, although the hard-core and energy contributions to the pressure differ individually in both phases. In the fcc

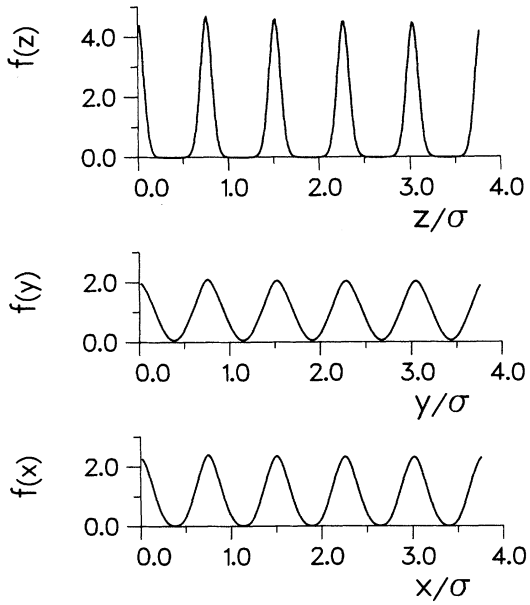

FIG. 7. Correlation functions $f(z)$, $f(x)$, and $f(y)$ [Eq. (7)] for dipolar hard spheres at $\rho^*=1.138$, $\mu^*=2.5$, and $\epsilon'=\infty$ (fcc).

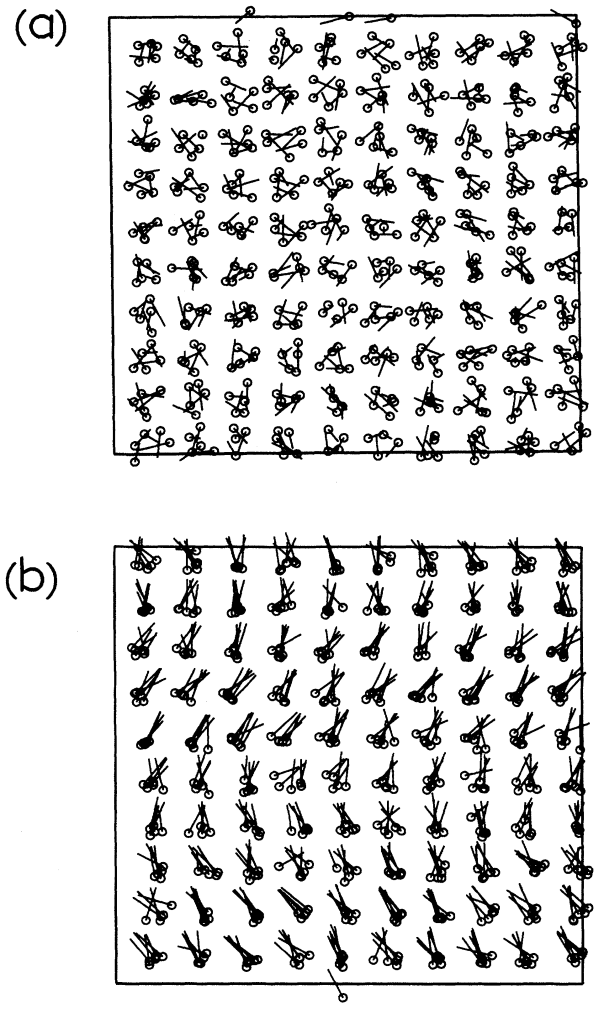

FIG. 8. Snapshot of a configuration of 500 dipolar hard spheres at $\rho^*=1.138$, $\mu^*=2.5$, and $\epsilon'=\infty$ (fcc phase). Projections of the dipole moments on the (a) xy, (b) xz, and (c) yz planes of the periodic simulation cell. The symbols are as in Fig. 3. The snapshot reveals helical ordering of the dipole moments along the z axis. The dimensions of the simulation cell are $L_x=7.61\sigma$, $L_y=7.59\sigma$, and $L_z=7.59\sigma$.

phase the energy is higher, but the hard core pressure lower, than corresponding values in the bct phase at the same density (cf. Table I).

When the fcc solid at $\rho^*=1.084$ was expanded to a lower density, a transition to a different stable lattice structure was observed. This structure will be shown below to bear close similarity with the bct structure considered above but is body-centered orthorhombic I (bco) rather than tetragonal I (bct) [24]. Upon further expansion, this bco structure remains stable to a density $\rho^*=0.9$, at which the system makes a transition to the fluid phase. However, it was noted that, depending on initial conditions, the fcc crystal could also be stabilized at densities lower than 1.08. For example, an NpT calculation at $p^*=3.1$ gave, after 60 000 moves per particle, a final density $\rho^*=1.024$ and thermodynamic and structural properties compatible with those of the fcc phase (possibly metastable), indicating appreciable overlap of the density ranges of the fcc and bco phases.

The fcc-bco transition results from a change in direction of the preferential ordering of the dipole moments from the [001] to the [110] direction which induces a contraction of the system along the [110] direction until near contact of the hard spheres is obtained. The resulting lattice structure is shown schematically in Fig. 9 for an ideal lattice with lattice vectors ($\mathbf{a}'$, $\mathbf{b}'$, $\mathbf{c}'$) ($\mathbf{b}'$ and $\mathbf{c}'$ are parallel to the y and z axes of the simulation cell, respectively). The simulation cell dimensions L_x and L_y adjust in such a way that the lattice spacings $|\mathbf{a}'|$ and $|\mathbf{b}'|$ are equal ($\simeq L_y/5$), and the angle α of $\mathbf{a}'$ with the x axis is $\sim 11°5$ (i.e., $\sin\alpha \simeq \frac{1}{5}$; recall that 5 is the number of repetitions of the unit cells along each direction of the original fcc lattice). It is readily verified that with the latter conditions the periodic boundary conditions imposed on the simulation cell are preserved. Furthermore, with the choice of lattice vectors $\mathbf{a}''$, $\mathbf{b}''$, $\mathbf{c}''$, as shown in Fig. 9 ($\mathbf{b}''$ parallel to the z axis), it is easily recognized that the lattice can effectively be viewed as an orthorhombic I structure (we will show below that a tetragonal structure is impeded by the chosen boundary conditions).

A snapshot corroborating the preceding description is shown in Fig. 10 for the density $\rho^*=1.01$. The polarization of the spheres is parallel to the xy plane and chain formation occurs along the c'' direction. These chains are made more clearly visible by projecting on the xy plane the spheres of a single lattice plane (parallel to the xy plane) (cf. Fig. 11). Chain formation is also apparent from the longitudinal distribution function $g_{\parallel}(r_{\parallel})$ which consists of a series of sharp peaks separated by approximately one hard-sphere diameter (Fig. 12). The positional disorder observed parallel to the y axis [cf. Fig. 10(c)] is only apparent and does not reveal formation of columns in the y direction, as was prematurely suggested in Ref. [5]. Rather, it results from overlap of the particle positions (in projection on the yz plane) due to the displacements of the particles from their lattice sites.

The average distance between spheres in the chains has been found to be equal to 1.025σ and independent of density, similar to the bct result. Furthermore, the angle between $\mathbf{a}'$ and $\mathbf{a}''$ is also independent of density in order that the chain arrangement satisfies the periodic boundary conditions along the x direction. This fixes the value of a'' at 1.26σ. These two constraints imply that the density of the system depends only on the value of the lattice spacing b'' along the z direction. The value of b'' should be inversely proportional to the density and this is what indeed is observed. The ratio b''/a'' increases from 1.14 to 1.28 when the density varies from 1.066 to 0.947.

The energy of the bco lattice is slightly higher than the energy of the bct lattice, the pressure is somewhat lower, and the order parameters S and P are identical (cf. Table I). We recall that the bco phase destabilizes near $\rho^* \simeq 0.9$ in favor of the nematic phase.

The pair-distribution-function projections h^{110}, h^{220}, and h^{112} are compared in Fig. 4 for the fcc and bct structures ($\rho^*=1.08$) and in Fig. 2 for the bct and bco structures ($\rho^*=1.01$). As far as h^{110} and h^{220} are concerned, the differences reflect mainly the differences in the underlying lattice structures. These are quite small for the bct and bco lattices; in fact, the only significant differences (including h^{112}) occur in the region $2\sigma \le r \le 2.6\sigma$ as a result of slightly different lattice neighbor distances. The structural behavior in the fcc and bct lattices is similar only at short distances ($r \le 1.25\sigma$). In particular, in both cases, a negative minimum is found in h^{112} at $r \simeq 1.16\sigma$. The negative well is narrower for the fcc lattice.

B. $\epsilon'=1$

We now turn to the results obtained when surrounding an infinitely large spherical volume of periodic replica of the simulation cell by vacuum ($\epsilon'=1$). The difference

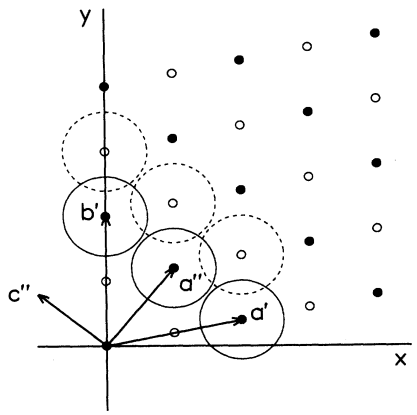

FIG. 9. Schematic representation (in the xy plane of the simulation cell) of the orthorhombic I (bco) lattice structure resulting from a deformation of the fcc lattice at densities $\rho^* \lesssim 1.06$. The lattice vectors $\mathbf{a}'$ and $\mathbf{b}'$ have equal length and the angle between them is such that the periodic boundary conditions imposed on the simulation cell are satisfied (see text). This lattice structure allows formation of chains along the c'' direction, where $\mathbf{a}''$, $\mathbf{b}''$, $\mathbf{c}''$ is a suitable set of convential lattice vectors characterizing the orthorhombic structure of the lattice ($\mathbf{b}''$ parallel to the z axis). The lattice positions marked by open and solid circles belong to lattice planes separated by a distance $b''/2$, respectively.

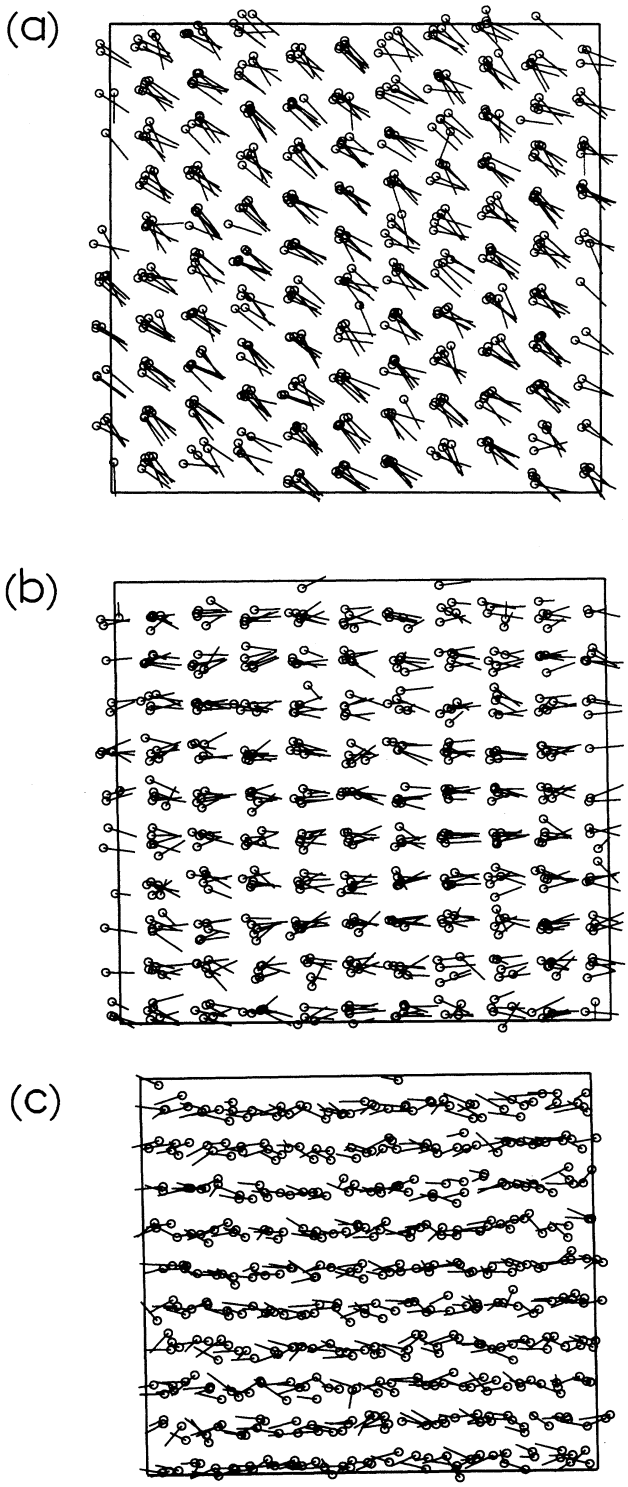

FIG. 10. Snapshot of a configuration of 500 dipolar hard spheres at $\rho^*=1.01$, $\mu^*=2.5$, and $\epsilon'=\infty$ (bco phase). Projections of the dipole moments on the (a) xy, (b) xz, and (c) yz planes of the periodic simulation cell. The symbols are as in Fig. 3. The dipole moments orient parallel to the xy plane. The bco lattice structure represented schematically in Fig. 9 is clearly visible in the xy projection. The dimensions of the simulation cell are $L_x=7.99\sigma$, $L_y=8.15\sigma$, and $L_z=7.67\sigma$.

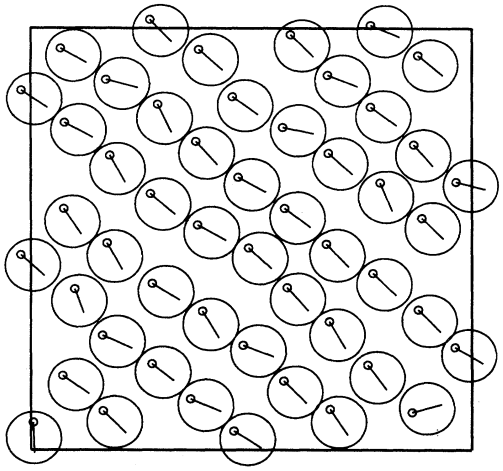

FIG. 11. Same as Fig. 10 but for hard spheres in one lattice plane parallel to the xy plane of the simulation box only. This snapshot demonstrates the formation of chains along the c'' axis of the bco lattice (cf. Fig. 9 and text). The dimensions of the simulation cell are $L_x=7.99\sigma$, $L_y=8.15\sigma$, and $L_z=7.67\sigma$.

with the conducting boundary conditions lies in an extra, positive term $2\pi\langle \mathbf{M}^2\rangle/3V$ in the Hamiltonian which represents the contribution to the energy from the depolarization field. For a perfectly polarized system, this energetically unfavorable term would be very large (in our case, $\sim 13N$, N being the number of particles) and would tend to destroy the ferroelectric order. From solid-state physics it is well known [24,25] that a possibility for the

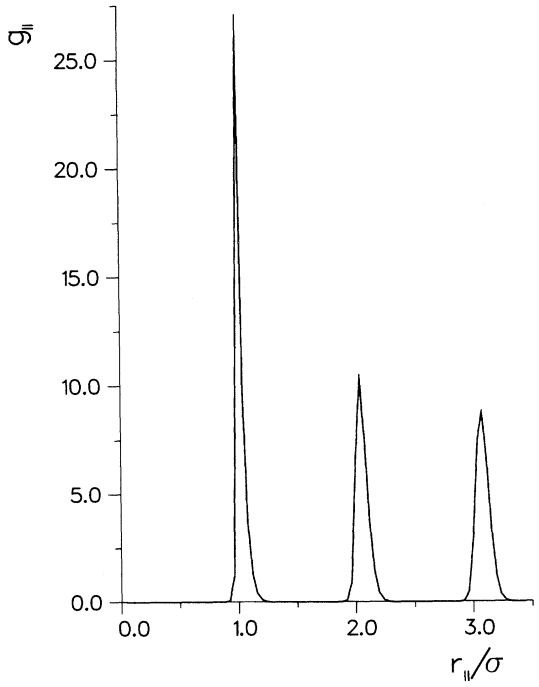

FIG. 12. Longitudinal correlation function $g_{\parallel}(r_{\parallel})$ [Eq. (8)] for dipolar hard spheres at $\rho^*=1.01$, $\mu^*=2.5$, and $\epsilon'=\infty$ (bco phase).

(macroscopic) system to reduce the effect of the depolarization field is to form domains, each domain being completely polarized but the directions of polarization of different domains not necessarily parallel.

A similar picture seems to emerge from the present calculations on a microscopic scale. We find that a 500–576 particle system splits into two (fluid and bct solid) or four (fcc solid) polarized "micro"-domains such that the total polarization of the system is zero. The calculations (NpT) performed for $\epsilon'=1$ are summarized in Table I. They were generally started from the final configuration (positions and orientations) of a previous run with $\epsilon'=\infty$, with the pressure fixed at the value obtained for $\epsilon'=\infty$. For densities $\rho^* \gtrsim 1.08$, both the fcc and bct lattices remained stable when ϵ' was changed from ∞ to 1. The polarization dropped rapidly to zero (after a few thousand trial moves per particle). The energy per particle increased slightly, but the pressure remained practically unchanged (due to a decrease of the hard-core contribution). A snapshot of the dipole moment arrangement in the fcc structure at $\rho^*=1.143$ is shown in Fig. 13. From this one can conclude (taking into account the periodic boundary conditions) that the system splits into four domains with polarizations parallel to the xy plane but pointing into different directions (roughly, the [110], [1−10], [−1−10], and [−110] directions of the simulation cell). In fact, due to the small system size the bulk parts of these domains have very limited extent in the y and z directions, and most particles of the system enter the formation of the domain walls which are quite gradual and easily recognizable by the vortex pattern of Fig. 13(c).

The angle-averaged PDF g^{000} is not much affected by the value of ϵ' (cf. Fig. 4). In contrast, for $\epsilon'=1$, h^{110} shows a tendency towards local dipolar alignment only over a range of r values of the order of the size of the ferroelectric domains, beyond which it decays to zero. This range is, of course, expected to depend greatly on system size [6].

The dipolar arrangement in the bct structure for $\epsilon'=1$ is shown in Fig. 14. A possible structure for the system to lower its polarization would have been to split into two domains with opposite polarizations along the chain axes. This is, however, not observed. Instead, one distinguishes two domains with polarizations parallel to a diagonal of the xy plane and thus perpendicular to the chain axes (Fig. 15). The chains are less well defined than in the system with $\epsilon'=\infty$. In the absence of strong attractive interactions along the z axis, the system has expanded in this direction (compared to the case $\epsilon'=\infty$), the average distance between sphere centers being now $\sim 1.06\sigma$. The order parameter S is rather high (~ 0.73), indicating a sharp domain interface.

For densities lower than 1.08, both the bct and bco lattices destabilized when ϵ' was changed from ∞ to 1 (maintaining, in the NpT calculations, the pressure fixed at the value found for $\epsilon'=\infty$). The system eventually melted and made a transition to a globally unpolarized state consisting of two ferroelectric domains with opposite polarizations. This process was generally very slow (a large pressure or density gap had to be bridged) and in

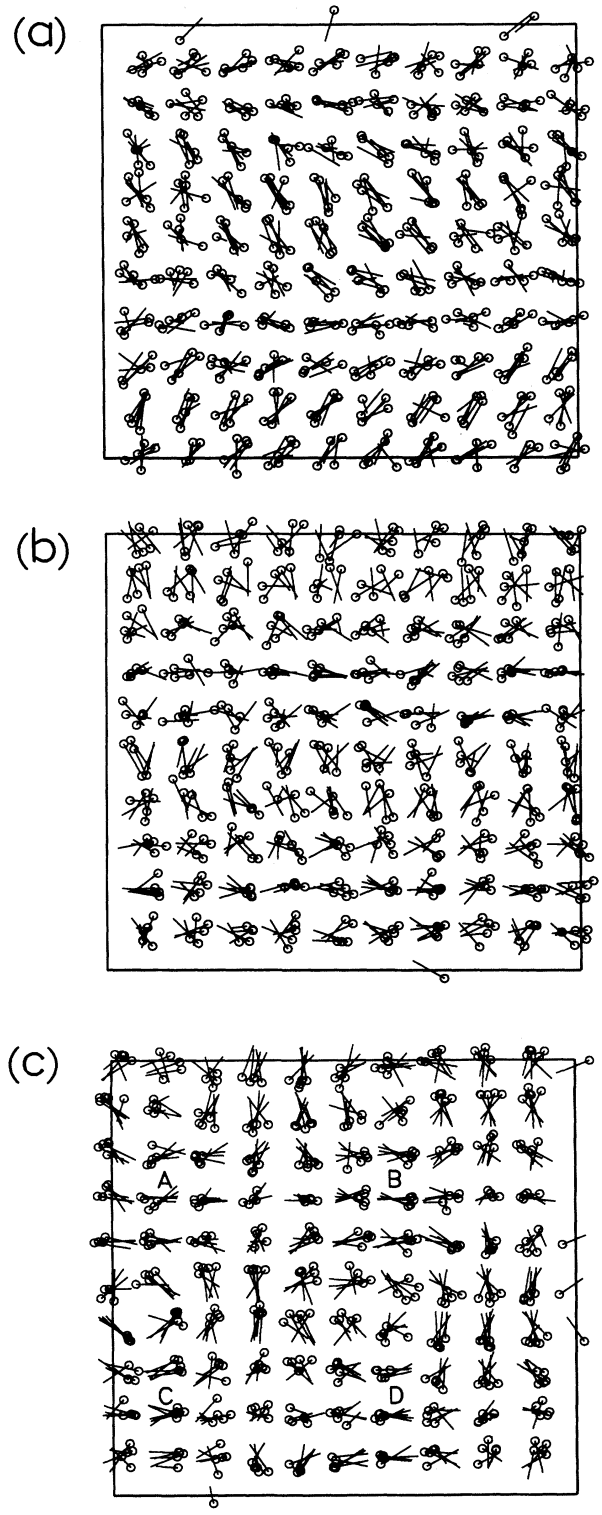

FIG. 13. Snapshot of a configuration of 500 dipolar hard spheres at $\rho^*=1.143$, $\mu^*=2.5$, and $\epsilon'=1$ (fcc phase). One clearly distinguishes four domains, denoted A, B, C, and D, respectively (taking into account the periodic boundary conditions), with different directions of the polarization (see text). The dimensions of the simulation cell are $L_x=7.68\sigma$, $L_y=7.52\sigma$, and $L_z=7.56\sigma$.

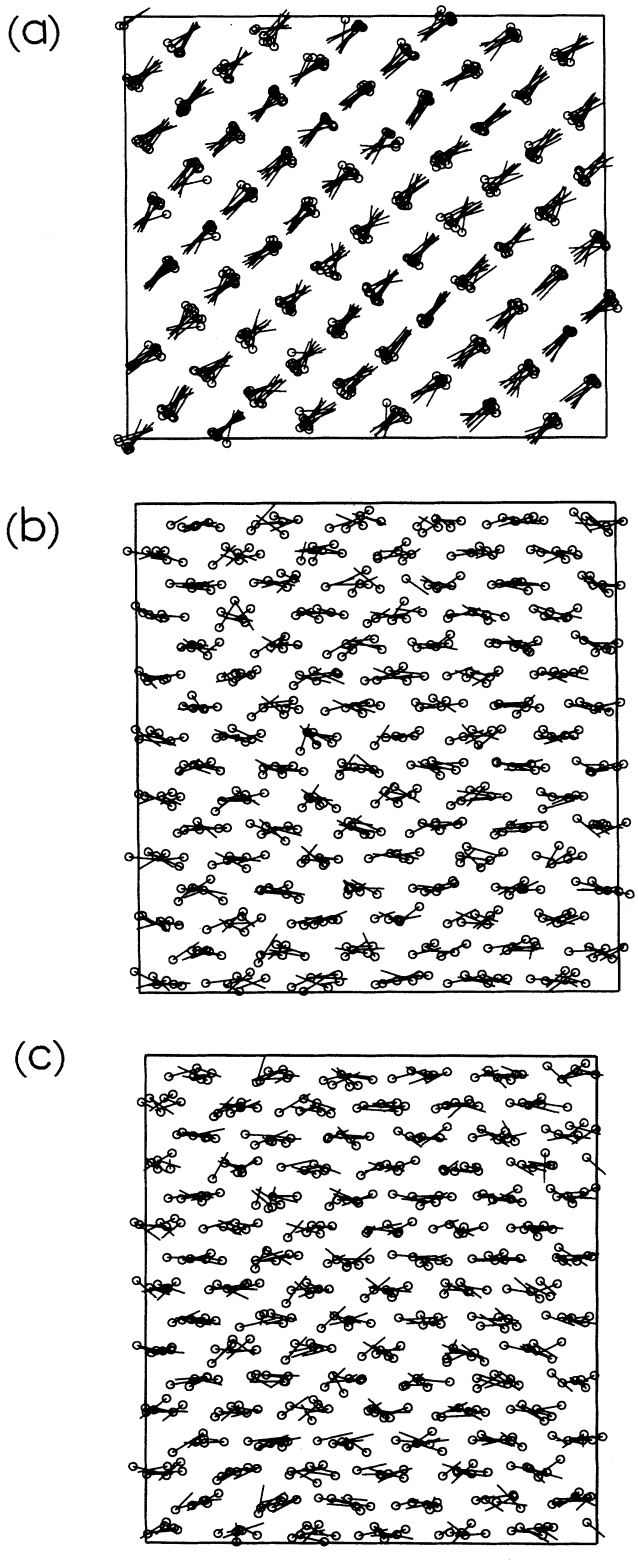

FIG. 14. Snapshot of a configuration of 576 dipolar hard spheres at $\rho^*=1.181$, $\mu^*=2.5$, and $\epsilon'=1$ (bct phase). One easily distinguishes two domains polarized in opposite directions along a diagonal of the xy plane. The dimensions of the simulation cell are $L_x=7.81\sigma$, $L_y=7.34\sigma$, and $L_z=8.49\sigma$.

most cases several hundred thousand trial moves per particle were necessary to reach equilibrium. For this reason we attempted to obtain fully converged results only in a few cases. Figure 16 provides a snapshot of the orientational order at $\rho^*=0.916$. This state was obtained starting from a bco configuration at $\rho^*=1.06$ and relaxing the system for 500 000 moves per particle. Two domains of roughly equal size are easily identified. In one domain, characterized by $1\sigma \le y \le 5\sigma$, the polarization is parallel to the xy plane and points in the [001] direction. The other domain is polarized in the opposite direction. Because of the orientational disorder in the interfacial region separating the two domains, the order parameter

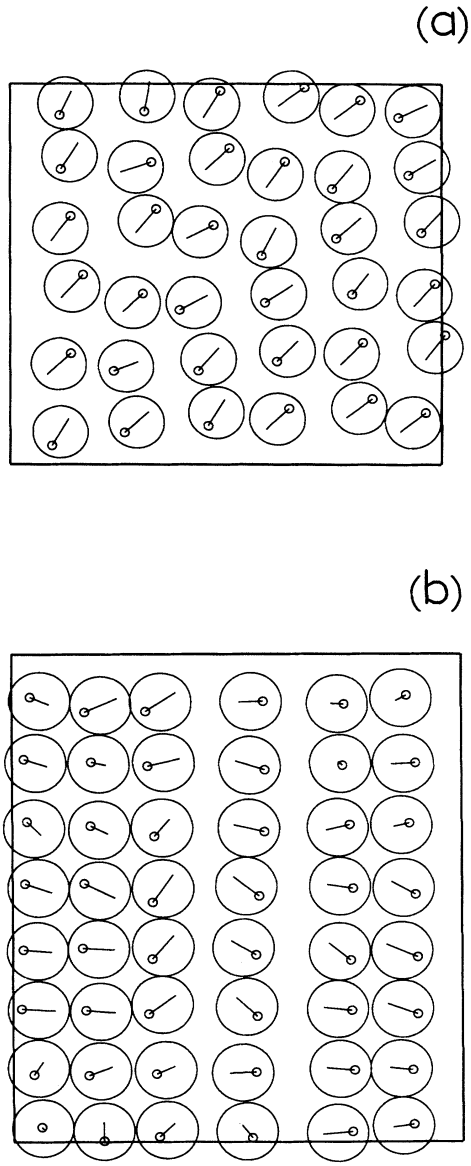

FIG. 15. Same as Fig. 14 but for hard spheres in one lattice plane parallel to (a) the xy plane and (b) the zy plane of the simulation cell. The dimensions of the simulation cell are $L_x=7.81\sigma$, $L_y=7.34\sigma$, and $L_z=8.49\sigma$.

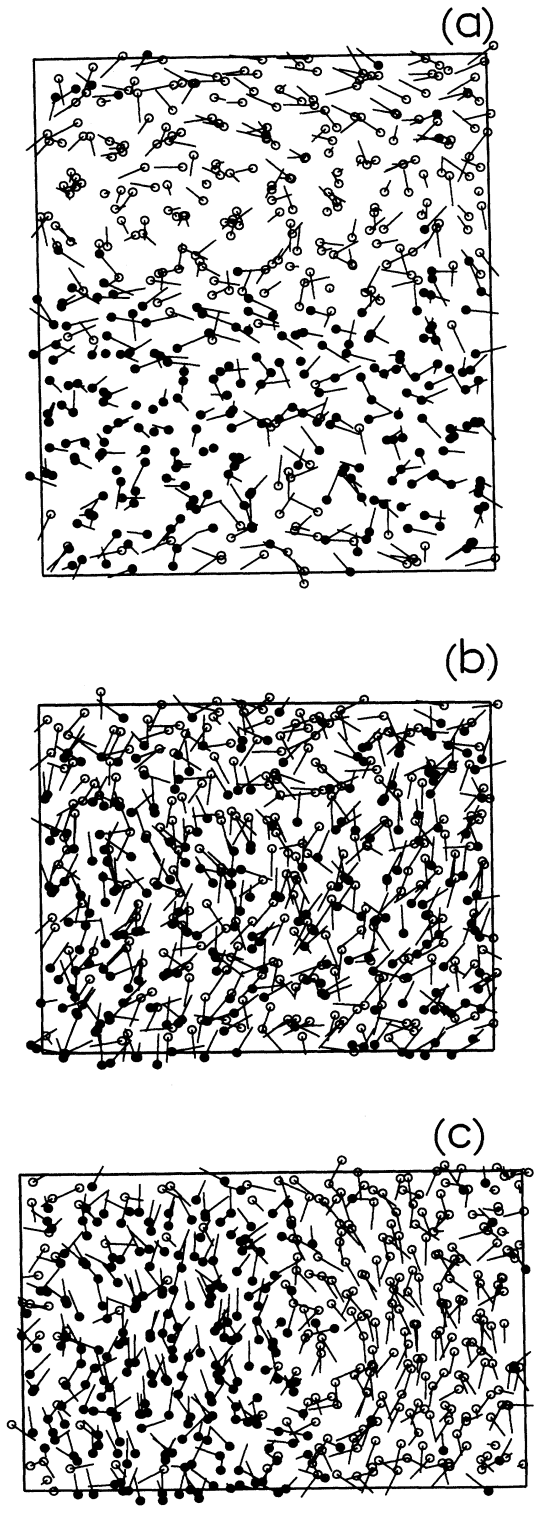

FIG. 16. Snapshot of a configuration of 500 dipolar hard spheres at $\rho^*=0.916$, $\mu^*=2.5$, and $\epsilon'=1$ (fluid phase). The system is seen to split into two domains with opposite polarizations along the z axis. Dipole moments pointing into the positive z direction are represented by an open circle, those pointing in the negative z direction by a solid circle. The dimensions of the simulation cell are $L_x=8.15\sigma$, $L_y=9.96\sigma$, and $L_z=6.71\sigma$.

S (~ 0.3) is much reduced with respect to its value in the ferroelectric state ($S\simeq 0.5$). More realistic values would be obtained by calculating an order parameter in the bulk part of each domain. Finally, we remark that a qualitatively similar picture arises when starting from a ferroelectric nematic state and changing ϵ' from ∞ to 1.

IV. SUMMARY

Monte Carlo simulations performed along the isotherm $T^*=0.16$ reveal that strongly interacting dipolar hard spheres can form orientationally ordered fluid and solid phases which, moreover, show ferroelectric behavior. Depending on the absence (conducting boundary conditions $\epsilon'=\infty$) or presence (vacuum $\epsilon'=1$) of a depolarization field, the system is uniformly polarized or splits into domains polarized in different directions with vanishing total polarization.

For the 500 particle system considered in this work, the transition from the isotropic to the nematic (ferroelectric) phase occurs at a density approximately equal to $\rho^*=0.7$, though this transition (system size dependence, order, etc.) has not been investigated in any detail. The fluid nematic phase is found to be stable up to a density ~ 1.0, possibly metastable at the highest densities, as suggested by appreciable overlap of the pressure curves of the fluid and solid phases. At higher density we investigated the stability of both the fcc and bct lattices. When $\epsilon'=\infty$, the bct lattice is characterized by fully polarized chains directed along the c axis and is stable over the whole density range 0.95–1.20 considered. A small asymmetry of the lattice spacings in the directions perpendicular to the c axis occurs nevertheless at the lowest densities. The fcc lattice is mechanically stable in the density range 1.02–1.20. The polarization is along a [001] direction, and in this direction the dipole moment orientations vary with helical order in going from one lattice plane to the other separated by one-half lattice spacing. Below $\rho^*\simeq 1.06$ (although, depending on initial conditions, a mechanically stable fcc phase was still found at $\rho^*=1.024$), the fcc lattice deforms in a way that enables chain formation along the [110] direction of the initial fcc lattice. From this perspective the new lattice structure is quite similar to the bct lattice mentioned above. However, it is orthorhombic rather than tetragonal, likely a consequence of the imposed parallelepipedic simulation cell and the periodic boundary conditions. At a density lower than $\rho^*\simeq 0.9$, the orthorhombic structure melts and the system forms a ferroelectric nematic phase.

At the present stage of investigation we are not able to tell which among these lattice structures is the most stable one, nor are we able to give a precise location of the ferroelectric nematic-solid transition. Answers to these questions must await detailed free-energy calculations which are, however, quite involved and beyond the scope of this work.

On turning ϵ' into 1, starting from a stable ferroelectric state at $\epsilon'=\infty$ and keeping p^* fixed, both the bct and fcc crystals remain stable for $\rho^*\geq 1.06$. The ferroelectric ordering splits into domains with different polarizations. For $\rho^*<1.06$, the depolarization field destabilizes the lat-

tice structure which melts and, at constant p^*, the system eventually goes towards an unpolarized fluid phase consisting of two roughly equal domains with opposite polarizations.

A study of the system size dependence of the domain formation, although of undeniable interest, has not been attempted here because of the substantial amount of computing time it would require. In Ref. [6] the view has been expressed that for sufficiently large samples the local orientational order in the ferroelectric domains would be quite similar to that obtained with small samples and $\epsilon' = \infty$. A result by Griffiths [26] supports this view. According to this result, the bulk free energy of a lattice of permanent dipole moments should be independent of sample shape in the thermodynamic limit (in the absence of an external electric field). In particular, needle-shaped (no depolarization field) and spherical specimens (depolarization field) in vacuum should have the same limit. Provided these results can be extended to off-lattice dipoles embedded into a hard core with periodic boundary conditions, both our results with $\epsilon' = \infty$ (no depolarization field) and $\epsilon' = 1$ (depolarization field) should be similar in the thermodynamic limit.

It is quite remarkable that both this work and the work of Wei and Patey, based on different short-range potentials and different simulation methods, lead, whenever comparable, to quantitatively similar results for the orientational structure of strongly interacting dipolar systems. Both works should be helpful in analyzing and understanding the structural properties of systems where dipolar forces play a dominant role.

ACKNOWLEDGMENTS

We thank G. N. Patey for communicating his work prior to publication. The Laboratoire de Physique Théorique et Hautes Energies is "associé au Centre National de la Recherche Scientifique."

[1] R. E. Rosensweig, Sci. Am. **247**, 124 (1982); *Ferrodynamics* (Cambridge University, New York, 1985).
[2] T. C. Halsey, Science **258**, 761 (1992); *Electrorheological Fluids,* edited by R. Tao (World Scientific, Singapore, 1992).
[3] A. T. Skjeltorp and G. Helgesen, Physica A **176**, 37 (1991).
[4] J. M. Caillol, J. Chem. Phys. **98**, 9835 (1993).
[5] J. J. Weis, D. Levesque, and G. J. Zarragoicoechea, Phys. Rev. Lett. **69**, 913 (1992).
[6] D. Wei and G. N. Patey, Phys. Rev. Lett. **68**, 2043 (1992); Phys. Rev. A **46**, 7783 (1992).
[7] See, e.g., M. P. Allen and D. J. Tildesley, *Computer Simulation of Liquids* (Clarendon, Oxford, 1989).
[8] S. W. de Leeuw, J. W. Perram, and E. R. Smith, Proc. R. Soc. London, Ser. A **373**, 27 (1980).
[9] P. G. Kusalik, J. Chem. Phys. **93**, 3520 (1990).
[10] J. Vieillard-Baron, Mol. Phys. **28**, 809 (1984); R. Eppenga and D. Frenkel, *ibid.* **52**, 1303 (1984).
[11] P. H. Fries and G. N. Patey, J. Chem. Phys. **82**, 429 (1985); L. Blum and A. J. Torruella, *ibid.* **56**, 303 (1972).
[12] J. W. Perram and M. S. Wertheim, J. Comput. Phys. **58**, 409 (1985).
[13] W. G. Hoover and F. H. Ree, J. Chem. Phys. **49**, 3609 (1968).
[14] M. Parrinello and A. Rahman, Phys. Rev. Lett. **45**, 1196 (1980); J. Appl. Phys. **52**, 7182 (1981).
[15] S. Yashanath and C. N. R. Rao, Mol. Phys. **54**, 245 (1985); D. Levesque, J. J. Weis, and P. Loubeyre, Phys. Rev. B **34**, 178 (1986).
[16] R. Tao and J. M. Sun, Phys. Rev. Lett. **67**, 398 (1991).
[17] R. Tao and J. M. Sun, Phys. Rev. A **44**, R6181 (1991).
[18] L. C. Davis, Phys. Rev. A **46**, R719 (1992).
[19] R. Tao, Phys. Rev. E **47**, 423 (1993).
[20] B. J. Alder, D. A. Young, M. R. Mansigh, and Z. W. Salzburg, J. Comput. Phys. **7**, 361 (1971); K. W. Kratky, Chem. Phys. **57**, 167 (1981).
[21] D. Frenkel and A. J. C. Ladd, J. Chem. Phys. **81**, 3188 (1984); K. W. Kratky, *ibid.* **82**, 5760 (1985).
[22] T. C. Halsey and W. Toor, Phys. Rev. Lett. **65**, 2820 (1990).
[23] T. Chen, R. N. Zitter, and R. Tao, Phys. Rev. Lett. **68**, 2555 (1992).
[24] C. Kittel, *Introduction to Solid State Physics* (Wiley, New York, 1971).
[25] N. W. Ashcroft and N. D. Mermin, *Solid State Physics* (Holt, New York, 1976).
[26] R. B. Griffiths, Phys. Rev. **176**, 655 (1968).